Ceramics International **21** (1995) 257–264

Solvent Debinding Kinetics of Alumina Green Bodies by Powder Injection Molding

Dah-Shyang Tsai* & Wei-Wen Chen

Department of Chemical Engineering, National Taiwan Institute of Technology, Taipei 10672, Taiwan

(Received 21 September 1994; accepted 24 October 1994)

Abstract: Solvent debinding of alumina green bodies shaped by powder injection molding is investigated. Debinding is carried out in normal hexane (n-C6), normal heptane (n-C7) and normal octane (n-C8), at 50, 60 and 80°C. Wax is the major constituent being leached. A shrinking core is observed at the early stage of 50°C solvent debinding. Debinding kinetics is adequately described by a single-parameter (effective diffusivity D_e) model except in the region of the core. The effective diffusivity decreases with the increase of carbon number of solvent from $5{\cdot}2 \times 10^{-6}$ (n-C6) to $3{\cdot}5 \times 10^{-6}$ cm^2/s (n-C8) at 50°C and from $6{\cdot}2 \times 10^{-6}$ (n-C6) to $3{\cdot}8 \times 10^{-6}$ cm^2/s (n-C8) at 60°C. For each solvent, the effective diffusivity is proportional to (leaching temperature/solvent viscosity). A core of clear edge not removed by solvent leaching could cause cracks in the subsequent processing steps. Cracks are observed around the edge of core after thermal debinding.

INTRODUCTION

Removal of fully loaded organics has been an obstacle for powder injection molding (PIM) processing, especially for objects of thick sections. Thermal debinding is widely used as the major means to remove organics before sintering. The evaporation of degradation products can cause pressure buildup within the green body and create voids at its center, bloating and cracks at its surface if thermal debinding is carried out hastily.[1–4] Long debinding time, therefore, is necessary to avoid these debinding flaws. Progressive binder removal is a valuable concept which is often taken into consideration in deciding a binder recipe for PIM. Constituents of low molecular weight are designed to be removed first. The constituent of much higher molecular weight will hold the integrity of the green piece after the removal of short-chain components. The early removal of low molecular weight constituents (>30 vol%) provides open channels for the diffusion of constituents pyrolyzed in higher temperatures and eases the pressure buildup.[5]

Solvent debinding takes advantage of the high solubility of low molecular weight constituents in organic solvents. The leaching or extraction of one binder component creates porosity in green bodies. A large amount of open porosity, after solvent debinding, allows the degraded products to diffuse to the surface easily. Therefore the thermal removal of insoluble binder components will be finished in a much shorter period without endangering the integrity of the green piece. The combination of solvent debinding and thermal debinding can be time saving.

White and German found that a higher powder loading needed a longer solvent debinding time to remove the wax in the binder. They attributed the longer debinding time to the difficulties of diffusion through smaller pores.[6] Lin and German studied the debinding of PIM parts by the condensed C7 solvent and used a diffusion model to describe the wax removal process.[7] Kankawa *et al.* studied the solvent debinding of PIM Fe–36%Ni using polyvinylbuthyral as binder and found very little residual carbon after thermal debinding.[8]

The effects of solvents and temperature on kinetics of solvent immersion debinding are the

*To whom correspondence should be addressed.

Ceramics International 0272-8842/95/$9.50 © 1995 Elsevier Science Limited, England and Techna S.r.l. Printed in Great Britain

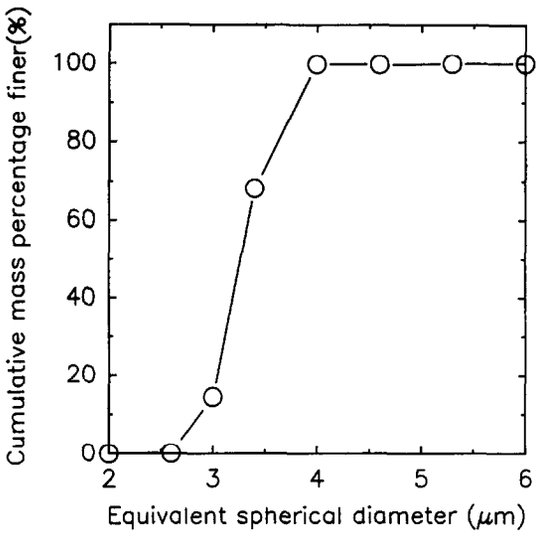

Fig. 1. Particle size distribution of alumina powder used in PIM.

subjects in this paper. A one-parameter model is utilized to describe the binder distribution during solvent debinding and evaluate the debinding kinetics quantitatively. The relation between solvent debinding and its subsequent thermal debinding is discussed.

EXPERIMENTAL

All green bodies were 1 cm in diameter, 8cm long cylinders, fabricated in one batch. The organic vehicle included three constituents; polypropylene (grade SA868M from Taiwan Polypropylene Co., Taiwan), paraffin wax (Merck) and stearic acid (Merck). The particle size distribution of α-alumina powder (AES11C from Sumitomo, Japan) is shown in Fig. 1. The formulation was 87 wt% (60 vol%) alumina, 7·8 wt% (24 vol%) wax, 4·42 wt% (13 vol%) polypropylene, 0·78 wt% (3 vol%) stearic acid. Ceramic powder and binder were mixed in a Z-type twinscrew blender at 180°C for 40 min. After mixing, the material was extruded into granules (3–5 mm), which served as the feedstock for injection molding.

The injection molding machine was an Arburg A270-210-500 (Germany). The barrel temperature was set at 130–135–140–145°C feed to the nozzle. The mold temperature was set at 100°C. The initial injection pressure was 1400bar, the first hold pressure was 1800bar (5 s), the second hold pressure was 1900 bar (3 s). The locking force was 300kN.

Leaching operations were carried out in a 1000 ml beaker that contained 700ml solvent. The cylinder immersed in solvents was held by a piece of nylon screen. The beaker, capped by a cover glass and sealed by Teflon, was kept at 50, 60 or

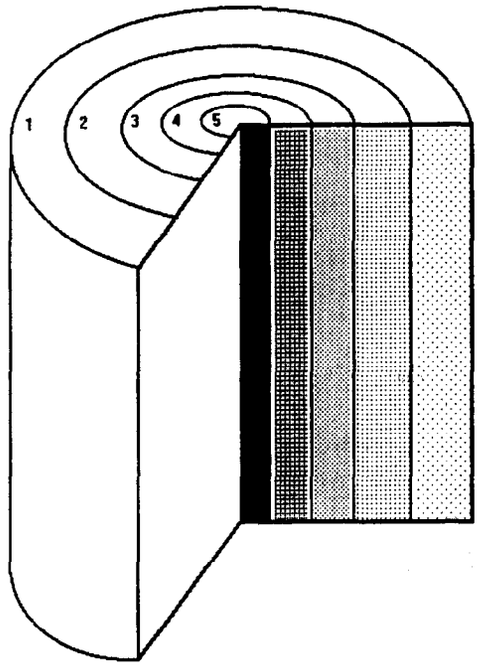

Fig. 2. Schematic diagram of sampling positions in determining the binder concentration profile.

80°C by a water bath. The cylinder was taken out of the solvent and dried for a day after leaching for several hours. Two ends of the cylinder were cut off to eliminate the end effects. A cylindrical piece, about 2 cm long, was taken from the middle section. Five concentric circles with equal spacings were drawn on the cross section of the short cylinder, as shown in Fig. 2. The solid portion between two concentric circles was carefully scraped off by a razor. The scraped powder was collected and mixed for TGA measurement of binder concentration. Five average binder concentrations were determined at r/R = 0·1, 0·3, 0·5, 0·7, 0·9. TGA analysis (sample 100 mg) was performed by a TGD-7000 thermal analyzer (Sinku-Riko, Japan) in air with a heating rate of 10°C/min up to 1000°C. A portion of leachant was filtered and subject to liquid chromatograph analysis (Spectro-Physics SP8800, USA).

MATHEMATICAL MODELING

Consider the binder in an infinitely long cylinder with radius R being leached by a large amount of solvent. Since the ceramic powder is inert during leaching, the binder concentration is defined as the ratio of binder weight over ceramic weight. Let C_0 represent the initial binder concentration, C_e be the equilibrium binder concentration, and C be the local binder concentration. Therefore, C_o–C_e is the total soluble binder concentration. Assume that diffusion of the soluble binder through the cylinder is the rate determining step, and the

binder is rapidly dried and fixed at its position after being taken out of the solvent. The binder concentration of leachant is assumed to be zero throughout the leaching operation. A partial differential equation with an undetermined parameter (effective diffusivity D_e) is established to describe the kinetics of the leaching operation.

$$\partial C/\partial t = (D_e/r)\,[\partial/\partial r(r\partial C/\partial r)] \qquad (1)$$

with boundary conditions $r = R$, $C = C_e$ and $r = 0$, $\partial C/\partial r = 0$; and initial condition $t = 0$, $C = C_0$. Its analytical solution is provided by Crank.[9]

$$\frac{C - C_e}{C_0 - C_e} = \sum_{n=1}^{\infty} \frac{2}{\lambda_n J_1(\lambda_n)} \exp(-D_e t \lambda_n^2/R^2) J_0(\lambda_n r/R) \qquad (2)$$

where $J_0(x)$ is the Bessel function of the first kind of order zero, λ_n is a root of $J_0(x) = 0$. $J_1(x)$ is the Bessel function of the first order. For a particular set of solvent and leaching temperature, the initial binder concentration, the equilibrium binder concentration ($t \to \infty$), and three binder concentration profiles in between were determined by the experimental procedure mentioned above. The correlation of D_e undergoes the following procedure. Taking the first term of the series solution of eqn (2) at $r/R = 0.5$ and neglecting the rest, eqn (2) becomes

$$\ln[((C-C_e)/(C_0-C_e))\,(\lambda_1 J_1(\lambda_1)/2)/J_0(\lambda_1 r/R)] = -(\lambda_1^2 D_e/R^2)t \qquad (3)$$

Three experimental data of $(C-C_e)/(C_0-C_e)$ at $r/R = 0.5$ were substituted into $\ln[((C-C_e)/(C_0-C_e))\,(\lambda_1 J_1(\lambda_1)/2)/J_0(\lambda_1 r/R)]$ and plotted versus $(\lambda_1^2/R^2)t$. The slope of the straight line is an approximate value for the effective diffusivity. Then this approximate value for D_e is further adjusted to better correlate the binder concentrations at other positions and times.

RESULTS AND DISCUSSION

Solubilities of wax and stearic acid

Table 1 lists the solubilities of wax and stearic acid in n-C6, n-C7 and n-C8 at 50 and 60°C. The solubility of wax increases significantly with temperature, and increases slightly with the carbon number of the solvent. Stearic acid is more soluble than wax in these solvents at 50°C. The solubilities of stearic acid become very large at 60°C and difficult to measure, since 60°C is close to its melting point. The solubility parameter δ of stearic acid is 7·9H, and δ of n-C6, n-C7 and n-C8 are 7·3H, 7·4H and 7·6H, respectively, at 25°C.[10] The difference of the solubility parameter between stearic acid and the solvent is reducing with increasing carbon number. The solubility of stearic acid in these three solvents, therefore, increases with the carbon number. Polypropylene swells slightly, but does not dissolve in n-C6, n-C7 or n-C8 at 50, 60 and 80°C. Both wax and stearic acid melt at 80°C.

Table 1. Solubilities of wax and stearic acid in normal hexane, heptane and octane

	n-C6	n-C7	n-C8
50°C	80g/100 g	90g/100 g	95g/100 g (wax)
	210g/100 g	270g/100 g	340g/100 g (S.A.)
60°C	270g/100 g	270g/100 g	290g/100 g (wax)
	N.A.	N.A.	N.A. (S.A.)

*The solubility is expressed as Xg solute/100g solvent.

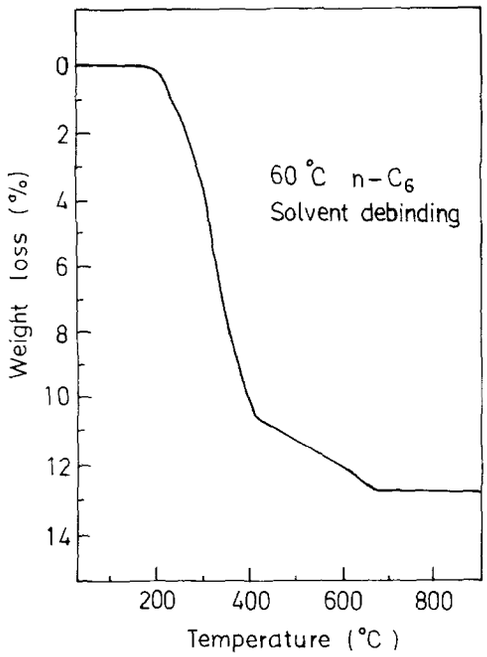

Fig. 3. A typical thermogravimetric curve of PIM sample.

Binder concentration from TGA

The binder concentration in the green body at each position is determined by TGA. A typical thermogravimetric curve is plotted in Fig. 3. There are two distinct weight loss regions in Fig. 3, a low temperature loss region (ca. 200–400°C) and a high temperature region (ca. 400–700°C). A major contribution to the weight loss in the low temperature region is due to the degradation of wax and stearic acid. Most of the weight loss in the high temperature region is caused by the decomposition of polypropylene. Unfortunately, due to considerable overlapping, it is difficult to separate the wax contribution from the polypropylene contribution in the TGA curve (even if stearic acid is neglected). Although we are unable to quantitatively determine the individual amount of each

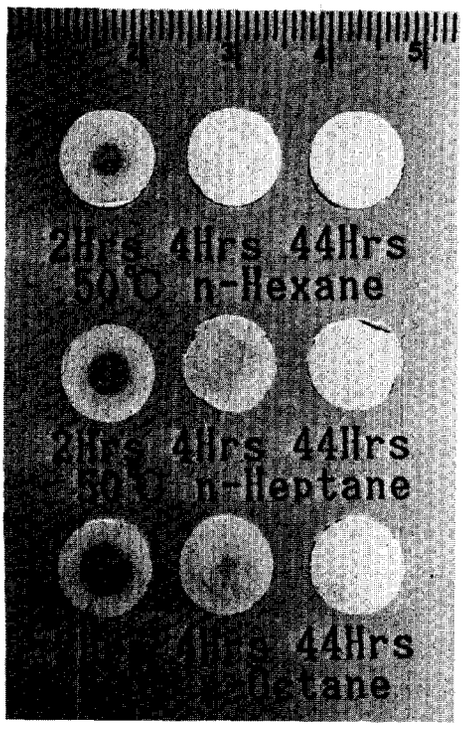

Fig. 4. Photograph of cross sections of cylinders leached for 2, 4 and 44 h in 50°C in n-C6, n-C7 and n-C8. Note the core-and-shell configurations of 2 h.

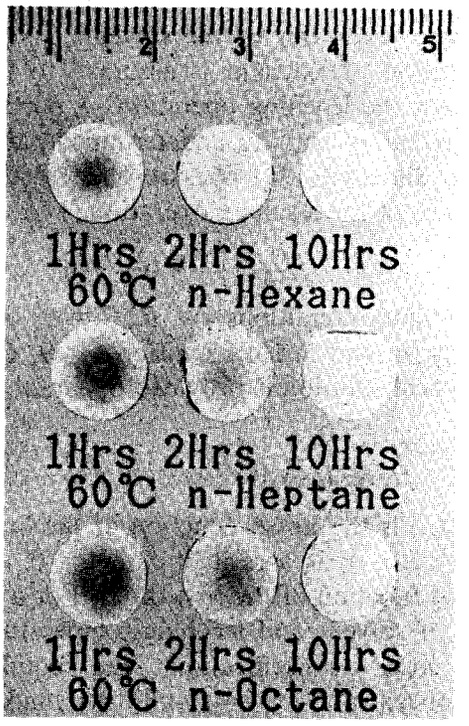

Fig. 5. Photograph of cross sections of cylinders leached for 1, 2 and 10 h at 60°C in n-C6, n-C7 and n-C8. Note the core-and-shell configurations of 1 h become diffuse.

component from the TGA result, the analysis of liquid chromatograph provides evidence that the major constituent in the leachant is wax.

Observation of shrinking core

Cores of clear edges are found in cylinders leached by n-C6, n-C7 and n-C8 at 50°C for 2 h, as illustrated in Fig. 4. The sizes of these cores, with diameters around 0·32 cm (n-C6), 0·42 cm (n-C7) and 0·48 cm (n-C8), increase with the carbon number of the solvent. After 4 h leaching, cores are removed by n-C6 and n-C7. A small core with diameter about 0·16 cm still remains after immersing in n-C8 for 4 h. The same trend is also observed in the cross sections of cylinders leached at 60°C, as indicated in Fig. 5. The size of the core after 1 h tends to be larger with a solvent of higher carbon number. Nevertheless, the cores at 60°C do not have clear boundaries between core and shell, and their diameters are difficult to measure. They are diffuse, blurred shadows, compared with their counterparts at 50°C. The shadows remain in 80°C leaching and are even more obscure, as shown in Fig. 6.

The removal process of soluble constituents in a green body can be viewed as a combination of two consecutive steps. The solvent first penetrates the binder phase and dissolves the soluble constituents, then the dissolved constituents diffuse through tortuous paths among the powder and leave the green body. When the diffusion of dissolved binder is much faster than the penetration of solvent, the binder diffuses out right after dissolution. There will be a step change in binder concentration at the interface of the core, and the

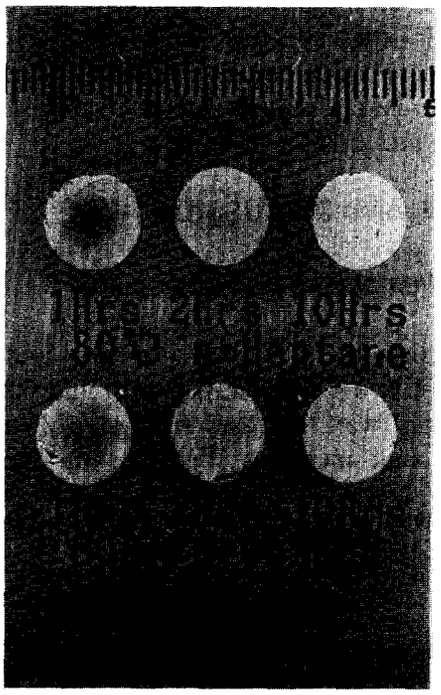

Fig. 6. Photograph of cross sections of cylinders leached for 1, 2 and 10 h at 80°C in n-C7 and n-C8. Note the core-and-shell configurations of 1 h are obscure.

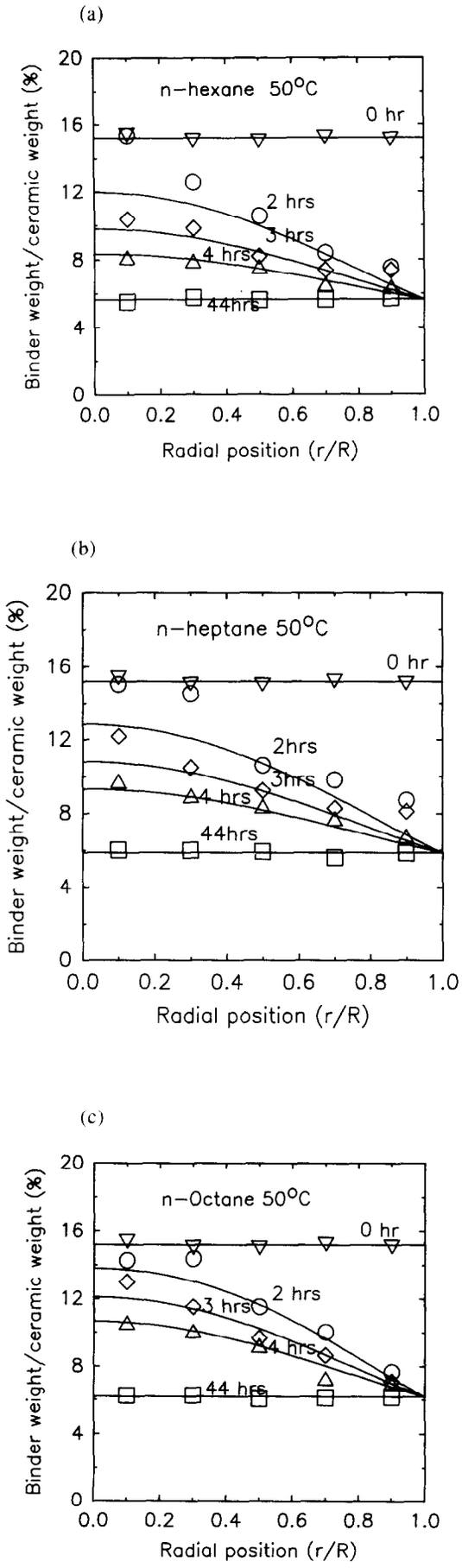

Fig. 7. Binder concentration profiles leached at 50°C in (a) n-C6; the solid lines are based on eqn (2) with $D_e = 5{\cdot}2 \times 10^{-6}$ cm^2/s; (b) n-C7; the solid lines are based on eqn (2) with $D_e = 4{\cdot}4 \times 10^{-6}$ cm^2/s; (c) n-C8; the solid lines are based on eqn (2) with $D_e = 3{\cdot}5 \times 10^{-6}$ cm^2/s.

binder concentration profile in the shell is flat. On the other hand, if the penetration of solvent is much more rapid, compared with the binder diffusion, the binder will be dissolved in the beginning, and slowly diffuse out. There will be a smoothly decreasing binder concentration profile. The continuous variation in shade from center to surface in Figs 5 and 6 indicates that the latter assumption is more appropriate for leaching at 60 and 80°C. A close examination of Fig. 4 reveals that these cores are surrounded by light shadows. These shadows imply that the binder concentration does not drop suddenly at the core interface. Therefore, 50°C leaching should be between the two extreme situations.

Binder concentration profile

Figures 7(a), (b) and (c) are plots of the binder concentration versus its radial position in the cylinder after leaching in n-C6, n-C7 and n-C8, respectively, at 50°C. The binder distribution before leaching (time = 0) is quite uniform. The average binder concentration is 15·2%. The binder distribution also reaches a uniform (equilibrium) value after immersion for a long time. The average binder concentrations are 5·64% (n-C6), 5·88% (n-C7) and 6·18% (n-C8) after 44 h. The final concentration increases with the carbon number of the solvent. This result appears to be inconsistent with the solubility results of wax and stearic acid. However, even if all wax and stearic acid in the cylinder are dissolved in the solvent, their concentrations are still well below their solubilities. The final binder concentration seems to be related to the solvent capability in separating out wax from the binder mixture, instead of wax solubility. The correlated effective diffusivities are $5{\cdot}2 \times 10^{-6}$ (n-C6), $4{\cdot}4 \times 10^{-6}$ (n-C7) and $3{\cdot}5 \times 10^{-6}$ (n-C8) cm^2/s. These values of D_e decrease with the increasing carbon number of the solvent.

A common feature among Figs 7 (a), (b) and (c) is that binder concentrations of 2-h leaching near the center of the cylinder are essentially equal to the initial concentration C_0, and these concentrations are not correlated by eqn (2). These regions of concentration C_0 are within $r/R < 0{\cdot}2$ for n-C6, $< 0{\cdot}4$ for n-C7 and n-C8. These sizes of concentration C_0 are quite close to the core sizes observed in Fig. 4 of the previous section. Presumably these regions are not penetrated by solvent, therefore, the proposed diffusion model fails to correlate these concentrations. It is logical to infer that these regions of C_0 will introduce errors in correlating the concentration profiles even after they vanish. If such errors exist, they do not seem to

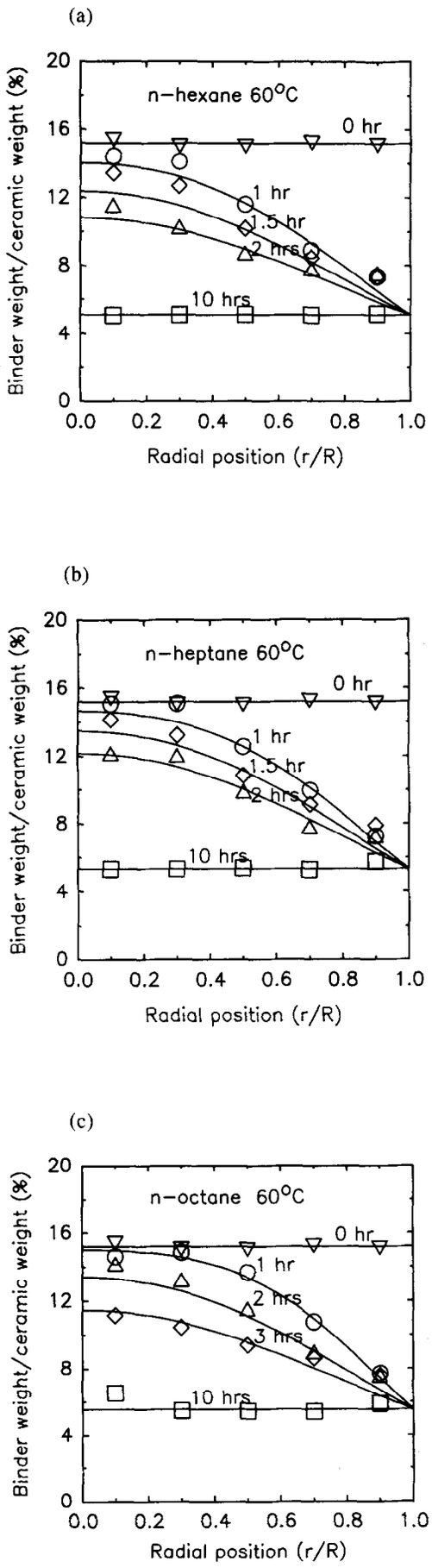

Fig. 8. Binder concentration profiles leached at 60°C in (a) n-C6; the solid lines are based on eqn (2) with $D_e = 6{\cdot}2 \times 10^{-6}$ cm^2/s; (b) n-C7; the solid lines are based on eqn (2) with $D_e = 4{\cdot}9 \times 10^{-6}$ cm^2/s; (c) n-C8; the solid lines are based on eqn (2) with $D_e = 3{\cdot}8 \times 10^{-6}$ cm^2/s.

bring in serious problems in correlating the rest of the data of 50°C leaching. Those binder concentration points, either after the cores disappear or outside the core regions, are well correlated by eqn (2).

Figures 8 (a), (b) and (c) are the binder concentration profiles after leaching in n-C6, n-C7 and n-C8 at 60°C, respectively. Equilibrium concentrations are 5·11% (n-C6), 5·40% (n-C7) and 5·55% (n-C8). Effective diffusivities are $6{\cdot}2 \times 10^{-6}$ (n-C6), $4{\cdot}9 \times 10^{-6}$ (n-C7) and $3{\cdot}8 \times 10^{-6}$ (n-C8) cm^2/s, higher than those D_e at 50°C. This is because the penetration rate is relatively faster at 60°C, and the diffusion becomes rate-limiting, as shown in Fig. 5. Deviations of experimental data from predicted values are less. The proposed model is able to correlate better as a whole.

Figures 9 (a) and (b) are the concentration profiles after leaching in n-C7 and n-C8 at 80°C. Effective diffusivities are $7{\cdot}6 \times 10^{-6}$ (n-C7) and 6·6

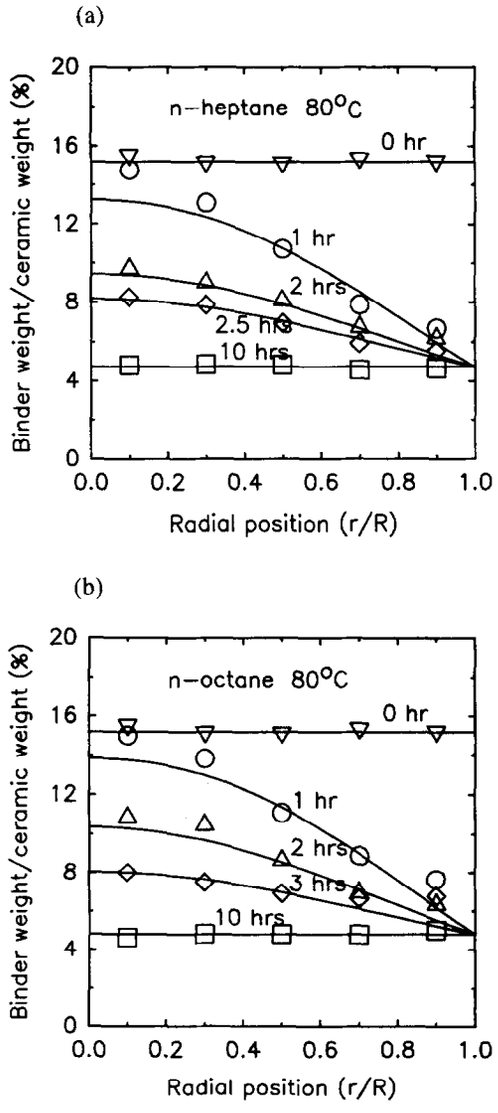

Fig. 9. Binder concentration profiles leached at 80°C in (a) n-C7; the solid lines are based on eqn (2) with $D_e = 7{\cdot}6 \times 10^{-6}$ cm^2/s; (b) n-C8; the solid lines are based on eqn (2) with $D_e = 6{\cdot}6 \times 10^{-6}$ cm^2/s.

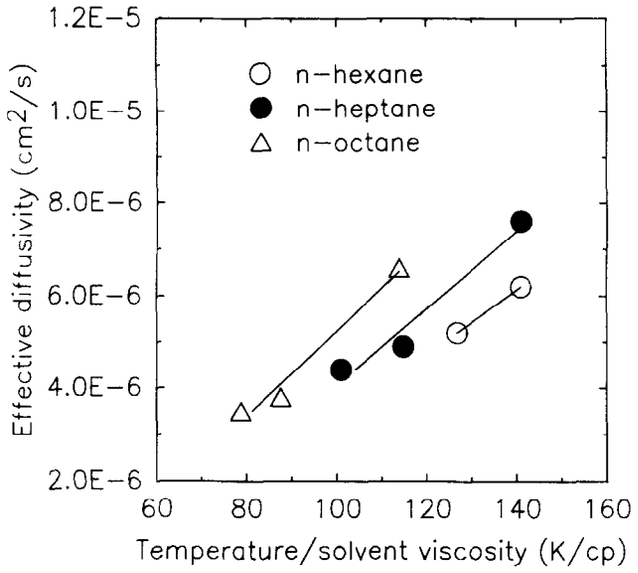

Fig. 10. Effective diffusivities versus leaching temperature/ solvent viscosity.

$\times 10^{-6}$ cm^2/s (n-C8). Equilibrium concentrations are 4·73% (n-C7) and 4·80% (n-C8). In general, effective diffusivity D_e decreases with the increasing carbon number of the solvent, and increases with the leaching temperature. Equilibrium concentration C_e increases with the carbon number of the solvent and decreases with the increasing leaching temperature.

Figure 10 indicates these effective diffusivities are roughly proportional to the ratio of leaching temperature/ solvent viscosity. The proportional constant is 6·99 $\times 10^{-8}$ for n-C6, 8·28 $\times 10^{-8}$ for n-C7 and 9·25 $\times 10^{-8}$ for n-C8, if the unit of D_e is cm^2/s, the unit for temperature is K, and the unit for viscosity is centipoise. The proportional constant increases with the molecular weight of the solvent. This result is consistent with the correlation equation proposed by Wilke and Chang for mutual-diffusion coefficients in dilute solutions, which is based on the classical Einstein–Stokes equation.[11,12]

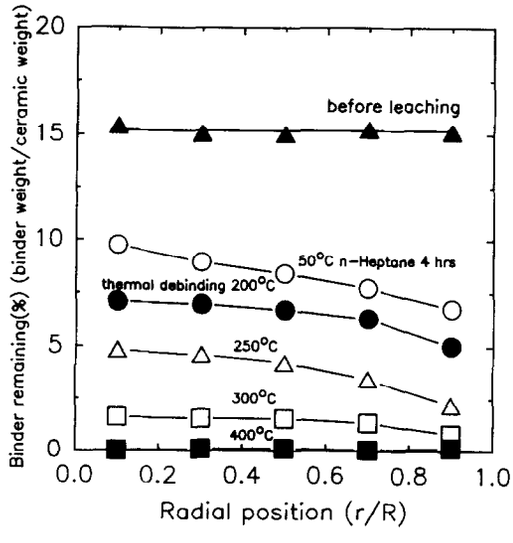

Fig. 11. The binder distribution after both solvent debinding and thermal debinding.

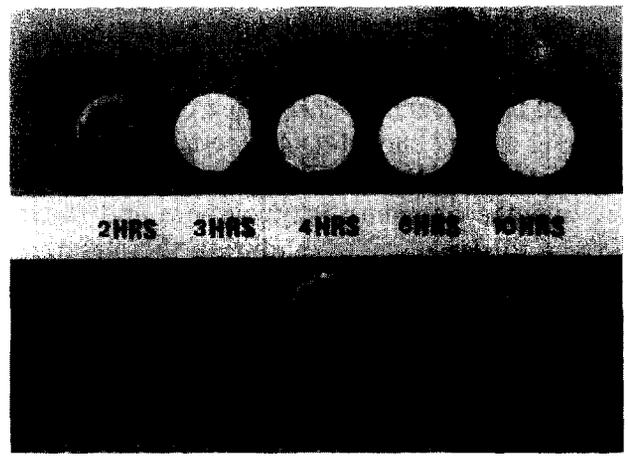

Fig. 12. Core-and-shell configurations and cracks around the boundaries. Cross sections at the lower row are leached in n-C7 at 50°C. Cross sections at the upper row are cylinders after leaching and 180°C thermal debinding for 30 min.

Although a higher temperature leads to a higher leaching rate, and the debinding operation appears to be more efficient at a high leaching temperature, a temperature that is too high, for example 80°C, often leads to cracks after leaching. The cracks are assumed to be associated with the swelling effect of solvent which increases with the temperature.

Figure 11 illustrates the binder concentration profile of a cylinder which underwent both solvent debinding and subsequent thermal debinding. Four cylinders were leached by n-C7 at 50°C for 4 h, then heated in a furnace at 200, 250, 300 and 400°C, respectively, for 1 h. Figure 11 indicates that 4-h solvent debinding in n-C7 plus 400°C thermal debinding can remove the organics completely. A debinding time of 5–6 h is much shorter than the time needed if only thermal debinding is applied. The green pieces after solvent plus thermal debinding can be sintered at 1600°C to over 95% theoretical density.

Core of clear edge as a crack source

The core-and-shell configuration formed in leaching seems to be related to the crack formation during its subsequent thermal debinding. Figure 12 illustrates the cross sections of cylinders after leaching for a certain amount of time at 50°C in n-C7 and their cross sections after further heating at 180°C for 30 min. The cross sections after leaching are dyed to emphasize the cores. These cylinders were molded in a different composition; Al_2O_3 87 wt%, wax 8 wt%, polypropylene 1·4

wt%, stearic acid 3·6 wt%. For those cylinders with clear cores after leaching, their cross sections show cracks around the edge of the core after thermal treatment. When the core disappears after leaching is long enough (>4 h), cracks will not be found. It seems that the boundary is a vulnerable site and the boundary between core and shell is subject to certain stresses during thermal treatment or handling. For those cylinders having diffuse shadows in the early leaching stage, no such cracks are found. It is wise to eliminate the core during leaching, then proceed with the thermal debinding.

CONCLUSIONS

The kinetics and mechanism of solvent immersion debinding is studied on a wax/polypropylene binder system. Wax is leached in n-C6, C7, C8 to generate pores for the subsequent thermal debinding. The major rate limiting factor of leaching is the diffusion of dissolved constituent through the porous green body. However, if the leaching temperature is lower than 50°C, the rate of solvent penetration into the binder phase might be a factor in determining the solvent debinding rate.

Cores of clear edges are observed at an early stage of 50°C leaching. The binder distribution in the green body is adequately described by a diffusion model with effective diffusivity as the single parameter, except in the core region. The effective diffusivity is proportional to (leaching temperature/solvent viscosity). The proportional constant increases with the molecular weight of the solvent. The interface between core and shell seems to be fragile, and it could be a source of cracks in the following processing steps.

ACKNOWLEDGEMENT

Partial financial support from the National Science Council of Taiwan, under contract number NSC83-04050-E011-038, is acknowledged.

REFERENCES

1. TSAI, D. S., Pressure buildup and internal stresses during binder burnout: numerical analysis. *AIChE J.*, **37** (1991) 547–54.
2. SHAW, H. M. & EDIRISINGHE, M. J., Removal of binder from ceramic bodies fabricated using plastic forming methods. *Amer. Ceram. Soc. Bull.*, **72** (1993) 94–9.
3. EDIRISINGHE, M. J., Binder removal from moulded ceramic bodies in different atmosphere. *J. Mater. Sci. Lett.*, **10** (1991) 1338–41.
4. MATAR, S. A., EDIRISINGHE, M. J., EVANS, J. R. G. & TWIZELL, E. H., The effect of porosity development on the removal of organic vehicle from ceramic or metal moldings. *J. Mater. Res.*, **8** (1993) 617–25.
5. SHUKLA, V. N. & HILL, D. C., Binder evolution from powder compacts: thermal profile for injection-molded articles. *J. Amer. Ceram. Soc.*, **72** (1989) 1797–803.
6. WHITE, G. R. & GERMAN, R. M., Dimensional control of powder injection molded 316L stainless steel using *in-situ* molding condition. *Metallurgy and Particulate Materials*, **5** (1993) 121–32.
7. LIN, S. T. & GERMAN, R. M., Extraction debinding of injection molded parts by condensed solvent. *Powder Met. Intern.*, **21** (1989) 19–24.
8. KANKAWA, Y., SAITOU, K., KANEKO, Y. & SASATANI, Y., Solvent debinding of injection molded Fe–36%Ni with use of polyvinylbuthyral as organic binder. *Powder and Powder Metallurgy*, **40** (1993) 531–5 (in Japanese).
9. CRANK, J., *The Mathematics of Diffusion*, 2nd edn. Oxford University Press, London, 1973, p. 73.
10. WEAST, R. C. (ed.), *Handbook of Chemistry and Physics*, 70th edn. CRC Press, Florida, 1989, c-681–c-683.
11. REID, R. C., PRAUSNITZ, J. M. & SHERWOOD, T. K., *The Properties of Gases and Liquids*, 3rd edn. McGraw-Hill, New York, 1977, pp. 542–5.
12. PERRY, R. H. & GREEN, D. (ed.), *Perry's Chemical Engineers' Handbook*, 6th edn. McGraw-Hill, New York, 1984, pp. 3-252.